CrossMark

Nanoscale zero valent supported by Zeolite and Montmorillonite: Template effect of the removal of lead ion from an aqueous solution

Nicolás Arancibia-Miranda [a],[*], Samuel E. Baltazar [b], Alejandra García [c],[d], Daniela Muñoz-Lira [a],[e], Pamela Sepúlveda [a], María A. Rubio [a], Dora Altbir [b]

[a] Facultad de Química y Biología, CEDENNA, Universidad de Santiago de Chile, USACH, Casilla 40, Santiago C.P. 33, Chile
[b] Departamento de Física, CEDENNA, Universidad de Santiago de Chile, USACH, Av. Ecuador 3493, Santiago 9170124, Chile
[c] CIMAV, S.C. Alianza Norte 202, Carretera Monterrey-Aeropuerto Km 10, C.P. 66600, Apodaca Nuevo León, Mexico
[d] University of Texas at San Antonio, Physics and Astronomy Department, One UTSA circle 78249, San Antonio, Texas, USA
[e] Facultad de Ciencias, Universidad de Chile, UCH, Las Palmeras 3425, Santiago 7800024, Chile

HIGHLIGHTS

- The Z–nZVI and Mt–nZVI composites showed a high efficiency in the removal of Pb^{2+} present in aqueous solutions.
- The fastest removal of Pb^{2+} was obtained with Mt–nZVI.
- The adsorption intensity increased 300 times in the composites, respect to the pristine materials.
- The magnetic behavior of the composites reveals a high presence of nZVI particles.
- These composites have potential industrial and environmental applications.

ARTICLE INFO

ABSTRACT

In this work, we have studied the Pb^{2+} sorption capacity of Zeolite (Z) and Montmorillonite (Mt) functionalized with nanoscale zero-valent iron (nZVI), at 50% w/w, obtained by means of an impregnating process with a solvent excess. The composites were characterized by several techniques including X-ray diffraction; scanning electron microscopy (SEM); BET area; isoelectric point (IEP); and, finally a magnetic response. Comparatively significant differences in terms of electrophoretic and magnetic characteristics were found between the pristine materials and the composites. Both structures show a high efficiency and velocity in the removal of Pb^{2+} up to 99.0% (200.0 ppm) after 40 min of reaction time. The removal kinetics of Pb^{2+} is adequately described by the pseudo second-order kinetic model, and the maximum adsorbed amounts (q_e) of this analyte are in close accordance with the experimental results. The intra-particle diffusion model shows that this is not the only rate-limiting step, this being the Langmuir model which was well adjusted to our experimental data. Therefore, maximum sorption capacities were found to be 115.1 ± 11.0, 105.5 ± 9.0, 68.3 ± 1.3, 54.2 ± 1.3, and 50.3 ± 4.2 mg g^{-1}, for Mt–nZVI, Z–nZVI, Zeolite, Mt, and nZVI, respectively. The higher sorption capacities can be attributed to the synergetic behavior between the clay and iron nanoparticles, as a consequence of the clay coating process with nZVI. These results suggest that both composites could be used as an efficient adsorbent for the removal of lead from contaminated water sources.

1. Introduction

The development of industrial processes has clearly affected our ecosystem over the last few centuries. For instance, water resources have been contaminated by several trace elements such as Pb^{2+},

Cu^{2+}, Cd^{2+}, $CrO_4{}^{2-}$, AsIII, and AsV [1–3], produced as residues from different industrial activities [4,5]. In particular, lead (Pb) is one of the most dangerous pollutants and it is widely spread throughout the world, where the main emission sources to the environment, especially to water resources, which come from anthropogenic activities, such as mine drainage, the disposal of batteries, and paint production [6–9]. The harmful effects of Pb have been well established in scientific literature, where many diseases such as anemia, chronic headaches and diarrhea have been diagnosed

when exposed to low concentrations of this metal [10]. Moreover, if humans are exposed to lead higher than $10\,\mu\mathrm{g}\,\mathrm{L}^{-1}$ [11], this contaminant could act as a powerful neurotoxic agent, leading to irreversible damage of the reproductive system along with hepatic and renal failure [10,12].

Nanoscale zero-valent iron (nZVI) is widely used for the removal of these pollutants, where their structural and surface characteristics such as surface area, size, and surface charge favor the sorption processes [2,3,7]. Due to Van der Waals and magnetic forces, nZVI suffers aggregation, and consequently, decreases their surface area and limits their sorption capacity [2,5–7]. This effect can be diminished through the immobilization of the nanoparticles inside different clay matrices such as Zr oxides, silica or polymeric cellulose acetate films, allowing nZVI to work under extreme conditions of pH and temperature as well as improving the sorption process [13–18]. Clays have an important removal capacity of heavy metals, Zeolites and Montmorillonites being some of the most studied materials [19–23]. Zeolites has been characterized as alkaline aluminosilicate, containing exchangeable cations (Na^+, K^+, Ca^{2+} and Mg^{2+}), along with water molecules coordinated in the structure [24,25]. On the other hand, Montmorillonite, is one of the most expandable minerals (Clay 2:1) characterized by its laminar organization, consisting of two tetrahedral layers of silica and a central octahedral layer of aluminum oxide [21,25–28]. Both possess a negative charge as a consequence of the isomorphous substitution process, providing a high cation-exchange capacity of ions [23–30]. In addition, the high porosity of clay is widely used in the removal of metallic ions present in aqueous solutions. This process occurs following two mechanisms: cation exchange (charge effect) and the formation of inner sphere complexes, due to the ionization of surfaces silanol sites ($\equiv$Si$-$OH) and aluminols ($\equiv$Al$-$OH) [18,29,30].

Nevertheless, the differences at a structural level and their physicochemical properties, (dimensions; surface area; surface charge; Al/Si ratio; cation-exchange capacity; and, chemical and mechanical stability) affect the size and aggregation of nZVI during the immobilization process, conditioning several parameters such as sorption velocity, capacity and affinity between composites and the studied analyte [8,17,31,32].

In this study we describe the synthesis and characterization of both composites, Mt–nZVI and Z–nZVI, and analyze the role of the structures of clays in the size, aggregation and reactivity of the immobilized nZVI. Furthermore, we determine, via sorption studies, the efficiency of both composites in the removal of Pb^{2+}.

2. Materials and methods

2.1. Materials and chemicals

The chemical reagents used in the study ($Fe(NO_3)_3\,9H_2O$, $Pb(NO_3)_2$ in water, HNO_3, NaOH, $NaNO_3$ and $NaBH_4$) were analytical grade (Merck). The sample containing the natural Zeolite, was collected from a mine located at $36^\circ\,16'S\,71^\circ\,40'W$, which was then ground and sieved with a sieve of 2 mm openings. The <2 μm size particles were separated by a sedimentation procedure [33]. In the case of Montmorillonite, it was supplied by Aldrich.

2.2. Preparation of the composite

The composites were prepared according to a procedure described by Wang et al. [15]. Briefly, 1.0 g of Zeolite and Mt were homoionized with $NaNO_3$ 0.1 M for one week, and finally treated in a freeze-drying process. The coating process had a theoretical 2:1 mixture of clay/nZVI (w/w), obtained by dissolving 1.0 g of $Fe(NO_3)_3\,9H_2O$ in a volume of 250 mL of degassed nanopure water. The mixture was treated with ultrasound for 30 min, and

then vigorously stirred at room temperature for 180 min. To ensure efficient reduction of Fe (II), 25 mL of 1.6 M $NaBH_4$ solution was added at $5\,\mathrm{mL}\,\mathrm{min}^{-1}$ while stirring. The black solid product was then separated from the solution using an ultracentrifuge (Sorvall RC-5C Plus) and washed five times with a (1:1) ketone/water solution (9000 rpm for 30 min) degassed to remove residual salts. The composites were finally stored in N_2-purged desiccators.

2.3. Characterization of the composite

In order to identify the samples, we developed an XRD analysis on a Shimadzu XRD-6000 diffractometer with graphite monochromator and CuKα radiation. Samples were characterized by a field emission scanning electron microscope (FE-SEM) model 200 Nova NanoSEM FEI Company. The operative conditions were performed at low vacuum conditions, Helix detector and 10–18 kV. The particles sizes were determined in the following way. A crosshair with orthogonal axes was placed at the center of each particle. The crosshair was adjusted to make one of the axes coincide with the longest dimension of the particle, and the diameter was then calculated as the average dimension along the two axes. Nitrogen isotherms were measured at 77 K using a Quantachrome Nova Station A. The surface area was calculated using the Brunauer–Emmett–Teller (BET) method. The magnetic response of the samples was investigated with a vibrating sample magnetometer (VSM) operated at room temperature with a maximum magnetic field of 1.2 Tesla, and a sensitivity of 10^{-4} emu. The isoelectric point (IEP) was determined by measuring the electrophoretic mobility of particles on a Zeta Meter ZM4 apparatus. About 100 mg of each sample was suspended in 200 mL of a solution with ionic strength 1.0 mM (NaCl). The IEP was obtained from the EM *vs* pH graph as the pH at which EM = 0.

2.4. Sorption experiments

The adsorbed amount of Pb^{2+} ions q_t ($mg\,L^{-1}$), per unit weight at time t, was calculated from the mass balance equation as shown in Eq. (1):

$$q_t = \frac{(C_0 - C_t)V}{(M)}, \tag{1}$$

where C_o is the initial concentration of Pb ($mg\,L^{-1}$), C_t is the concentration at time t, V is the volume (L) and M is the mass (g) of the materials. All experiments were carried out in triplicate.

2.4.1. Sorption studies of Pb^{2+}

The kinetic studies had 20 mL of a Pb^{2+} solution ($200\,mg\,L^{-1}$) in 0.01 M $NaNO_3$ (background electrolyte) mixed with 50 mg of composite in 50 mL polypropylene centrifuge tubes. The systems were mixed mechanically with glass rods at 300 rpm for 120 min. The concentration of Pb^{2+} in solution was determined at 5, 10, 20, 30, 45, 60, 90, 120, 150 and 180 min.

Adsorption isotherms were obtained by varying the initial Pb^{2+} concentration from 1 to $200\,mg\,L^{-1}$. The suspensions were then stirred continuously at room temperature ($25 \pm 2\,^\circ\mathrm{C}$) and a pH controlled value using 1 M NaOH or HNO_3, measured by an Orion (model 250A) pH meter. Sample aliquots collected were filtered with 0.22 μm syringe filters. The concentrations of Pb^{2+} in supernatant solutions were determined using an atomic absorption spectrometer THERMO.

2.4.2. Pseudo first-order kinetics (PPO)

The linear form of pseudo first order model can be expressed as (Eq. (2)):

$$\log(q_e - q_t) = \log(q_e) - \frac{k_1}{2.303}t, \tag{2}$$

where q_e and q_t correspond to the amounts of solute adsorbed at equilibrium and time t (expressed in $(mg\,g^{-1})$), respectively, and k_1 (min^{-1}) is a combination of adsorption (k_a) and desorption (k_d) constants [34–38].

2.4.3. Pseudo-second order kinetics (PSO)

The pseudo second-order rate expression, which has been applied for analyzing chemisorption kinetics from aqueous solution, is linearly expressed as Eq. (3) [36–40]:

$$\frac{t}{q_t} = \frac{1}{q_e{}^2 \cdot k_2} + \frac{1}{q_e}t, \tag{3}$$

where k_2 is the PSO adsorption rate constant $(g\,mg^{-1}\,min^{-1})$. This model can also be used to estimate the initial adsorption rate of the system, which is defined as $h = k_2\,q_e^2$ [34,40].

2.4.4. Intraparticle diffusion model (Weber–Morris model)

The Webber–Morris pore-diffusion model is a single-resistance model derived from Fick's second law of diffusion. The mathematical dependence of sorbate uptake (q_t) on $t^{1/2}$ is given by:

$$q_t = k_{int}t^{1/2} + C, \tag{4}$$

where k_{int} $(mg\,g^{-1}\,min^{-1/2})$ is the intraparticle diffusion constant and C is a constant related to the thickness of the surface layer [40,41].

2.5. Goodness-of-fit of removal kinetic model

The best fit among the kinetic models is assessed by the linear coefficient of correlation (r^2), the non-linear Chi-square (χ^2), and the square of residuals (R).

The Pearson's chi-square (χ^2) statistic was used to evaluate the best-fit of kinetic models to experimental data. Square of residuals (R) was also used as a measure of the differences between model-predicted values and the values actually observed from the experimental data.

The square of residuals can be defined as:

$$R = \frac{1}{2}\sum{}_{i=1}(C_{cal} - C_{exp})^2. \tag{5}$$

The chi-square test is given as:

$$\chi^2 = \sum_{i=1}^{N} \frac{\left(q_{(exp)} - q_{(cal)}\right)^2}{q(cal)}. \tag{6}$$

The subscripts "exp" and "cal" show the experimental and calculated values, respectively, and N is the number of observations in the experimental data [2]. The better the fit of the models to experimental data, the smaller the χ^2 value.

2.6. Adsorption isotherm models

2.6.1. Langmuir isotherm

This model assumes that the sorption occurs in a monolayer over a homogeneous surface with a finite number of active sites and similar adsorption energies. Also this model provides the saturation point and maximum adsorption of the system. The Langmuir model can then be represented by:

$$q = \frac{q_m K_L C}{1 + K_L C}, \tag{7}$$

where q_m $(mg\,g^{-1})$ is the maximum adsorption capacity, q $(mg\,g^{-1})$ is the amount of adsorbed Pb^{2+}, C $(mg\,L^{-1})$ is the equilibrium Pb^{2+} concentration and K_L is the Langmuir constant [42].

2.6.2. Freundlich isotherm

The Freundlich model is widely used to describe the adsorption of an analyte on a heterogeneous surface, where the physisorption, which occurs in several layers, and the chemisorption, occurring in a monolayer, can be associated to the different adsorption energies of the adsorbent sites [42]. The equation describing the Freundlich model is:

$$q = K_F C^{1/n}, \tag{8}$$

where C corresponds to the equilibrium concentration, K_F and n are Freundlich isotherm constants, related to adsorption capacity and adsorption intensity, respectively.

3. Results and discussion

3.1. Characterization of the composite

Fig. 1 shows the X-ray diffraction patterns of the studied materials, being displayed on the left and on the right hand sides respectively; (a) the initial samples: natural Zeolite and Mt; (b) functionalized composites: Z–nZVI, and Mt–nZVI and (c) Z–nZVI/Pb²⁺ and Mt–nZVI/Pb²⁺ composites after Pb²⁺ sorption. On the left hand side of Fig. 1(a), it corresponds to a well crystallized Zeolite, the sample has the peaks of Al–Mordenite structure (PDF: 00-049-0924) and no other significant phases. On the right hand side of Fig. 1(a), describing Mt, we have identified broadened characteristic peaks of Mt species, named Na–Mt structure ($Na_{0.3}(Al,Mg)_2Si_4O_{10}\,8H_2O$) and Illite–Mt ($KAl_4(Si,Al)_8O_{10}(OH)_4\,4H_2O$) at $2\theta = 26.7°$ and an additional peak at $28.2°$ belonging to SiO_2. The total content of iron in both clays, did not exceed 3 and 1% for the Zeolite and Mt respectively.

Below these XRD patterns, Fig. 1 shows the crystalline phases of composites samples (b), exhibiting the peak of Fe^0 located at $2\theta = 44.7°$ and associated to the nZVI immobilized on the surface of the composite. The main peaks of both clays Zeolite and Mt exhibit a lower intensity compared to the initial samples, a phenomenon already described in the literature [15,18]. Additionally, the X-ray pattern of Mt–nZVI exhibits peaks at $2\theta = 30.1°$ and $35.5°$ associated to the formation of Fe_3O_4, along with the broadened peaks of Zeolite, Na–Mt, Illite–Mt and SiO_2 (Fig. 1).

Finally, we present the XRD patterns after the exposure of the composites to Pb^{2+} (Fig. 1c). In the case of Z–nZVI/Pb²⁺ (left hand side) we observe a peak of Pb, located at $2\theta = 35.9°$, a diminished peak of Fe, while the composite did not change the crystalline degree of the sample after Pb^{2+} sorption, indicating that the removal process occurs through multiple mechanisms [3,14,15,35]. The results of Mt–nZVI/Pb²⁺ (right hand side) shows the suppression of some peaks of Mt and Fe_3O_4, as well as the identification of the diffraction peak of Pb around $2\theta = 35.9°$ [14]. These changes can be associated to the formation of amorphous phases of iron oxides as well as the structural changes of the functionalized Mt [35]. Table S1 summarizes the diffraction peaks found in the samples with their corresponding angles and interplanar distances.

The samples were also characterized by SEM microscopy to observe the morphological changes after the removal of Pb^{2+}. Fig. 2 exhibits SEM images of the microstructure of Z–nZVI and Mt–nZVI before and after Pb^{2+} sorption and their corresponding particle size distribution (inset for each case). For nZVI supported by Zeolite (Fig. 2a and c), the size distribution shows particles with diameters ranging between 36 and 116 nm with a mean value of 69.8 nm. These particles get larger after Pb^{2+} sorption, with diam-
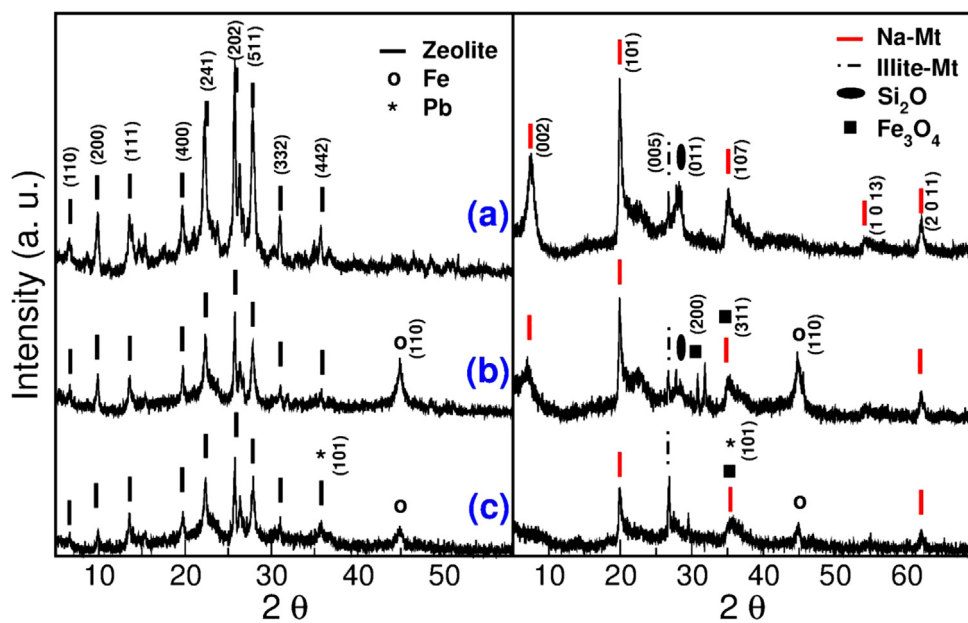
Fig. 1. XRD patterns of Zeolite (Z) and Montmorillonite (Mt) samples showing (a) the initial clays, (b) clays treated with nZVI particles and (c) treated clays after Pb^{2+} sorption.
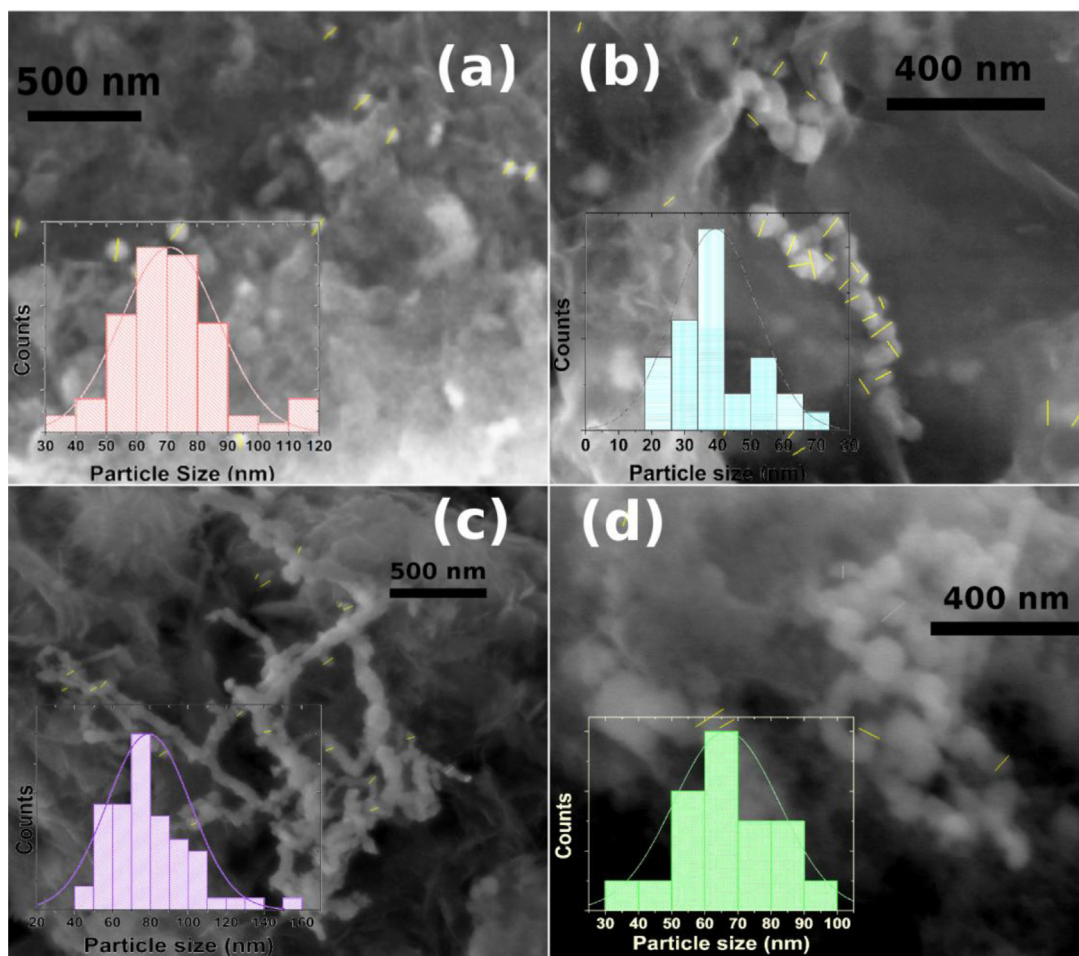

Fig. 2. SEM images of (a) Zeolite and (b) Mt doped with ZVI and (c,d) composites after Pb^{2+} sorption at pH 5.5 respectively. The particle size distribution of each sample is included as an inset ($n = 25$).

Table 1
Textural features of products.

Sample	Surface Area ($m^2\,g^{-1}$)	Pore Volume ($cm^3\,g^{-1}$)	Microporous volume ($cm^3\,g^{-1}$)	Average diameter (nm)
nZVI	24.7	0.104	0.011	16.9
Zeolite	31.0	0.071	0.015	9.1
Montmorillonite	8.2	0.063	0.004	30.5
Mt–nZVI	20.9	0.049	0.012	9.3
Z–nZVI	29.1	0.085	0.014	11.7

eters between 43 and 159 with a mean value of 76 nm. The nZVI on Mt particles (Fig. 2b and d) exhibit a wide size distribution with diameters between 19 and 70 nm, with an average of 37 nm, while the size of the particles after Pb^{2+} sorption range from 32 and 98 nm, with an average of 66 nm [16,17]. The increase of the particle size (see insets of Fig. 2) is mainly attributed to the formation of iron oxide/hydroxide and Pb compounds.

The BET area of the samples has shown $31.0\,m^2\,g^{-1}$ of natural Zeolite, which is slightly diminished after the nZVI doping to $29.2\,m^2\,g^{-1}$. The Pb sorption promotes an increase in the surface area of up to $67.7\,m^2\,g^{-1}$, mainly due to the oxidation of the nZVI. In the case of Mt, the BET area is $8.2\,m^2\,g^{-1}$, which is clearly increased after the nZVI doping ($20.9\,m^2\,g^{-1}$). Similarly, the lead sorption increases the measured BET area to $26.3\,m^2\,g^{-1}$. The enhancement in the surface area of Mt after the functionalization process with nZVI is due to an enhanced basal space of Mt. This effect is justified by the intercalation of Fe, a phenomenon reported for expandable clays [23] (Table 1).

The superficial behavior of the samples was described by electrophoretic mobility, a technique that is sensitive to the changes in composition that a surface may undergo, and the IEP is a good parameter for indicating what happens on the surface of the clays as a result of, for example, partial coverage by nZVI. Both clays present a negative charge over a wide pH range, however, the IEP was determined only with Zeolite (2.3 ± 0.1). The IEP of nZVI was 7.7 ± 0.2, which is a characteristic of this material [7]. The IEP results show values of 6.0 ± 0.1 for Z–nZVI and 4.5 ± 0.3 for Mt–nZVI (see Fig. 3), which means that the functionalization process drastically modifies the clay charges [18].

We obtained the magnetization response for an external magnetic field H. Fig. 4 illustrates the magnetic hysteresis of Z–nZVI and Mt–nZVI after the Pb^{2+} sorption process. Similar results have been reported in recent sorption experiments of AsO_4^{3-} y Pb^{2+} using nZVI [35,43]. The coercive fields (Hc) of both samples were
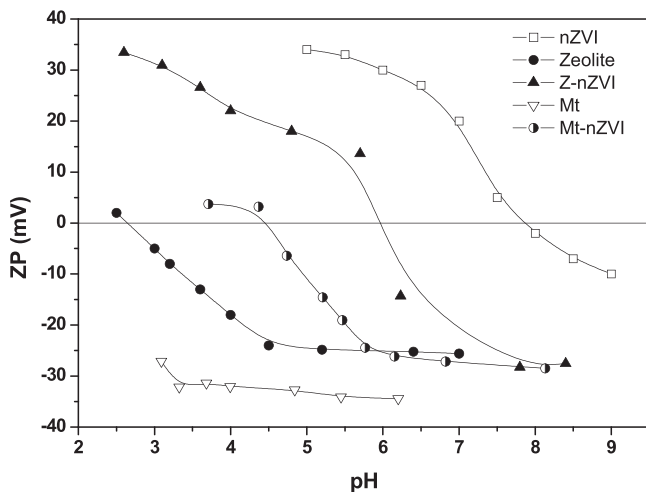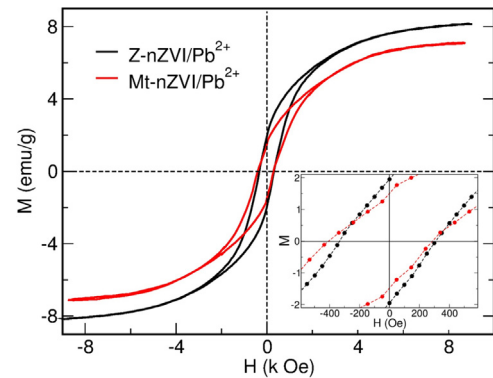
Fig. 4. Magnetization response of the nZVI-doped composites after Pb^{2+} sorption. The inset shows the behavior at low magnetic fields.

obtained at room temperature, being *ca.* 320 Oe and 340 Oe for Z–nZVI and Mt–nZVI, respectively (see inset in Fig. 4). In contrast, the remanence of Z–nZVI/Pb^{2+} was $1.9\,emug^{-1}$, a slightly higher result than the $1.5\,emu\,g^{-1}$ found for Mt–nZVI/Pb^{2+}. Also the saturation of the magnetization for Z–nZVI/Pb^{2+} obtained after an applied magnetic field of 8000 k Oe was $8.1\,emu\,g^{-1}$, which is higher than the $7.1\,emu\,g^{-1}$ of Mt–nZVI/Pb^{2+}. These results suggest an important formation of iron oxides in the case of Mt compared to Zeolite samples, which is supported with the spectra observed from XRD analysis. These results can be associated to a different oxidation of nZVI inside Mt respect to the oxidation process of Z–nZVI (Fig. 4).

3.2. Removal studies

In order to evaluate the impact of pH on the Pb^{2+} sorption, several studies were performed in batch, with a pH range of 3.0–6.0, being Pb^{2+} and $Pb(OH)^+$ the dominant species. At this pH range, precipitation is not the main removal process [44,45]. The Pb^{2+} sorption results with clays were slightly favored at high pH values, a result consistent with the obtained ZP measurements, where the Zeolite and Mt charges become negative as the pH is increased, due to the ionization of $\equiv Si-OH$ and $\equiv Al-OH$ groups, located at the edge of these substrates (Fig. 5) [17,18]. In the case of nZVI, an increase of the pH strongly diminishes the lead sorption, possibly due to the passivation process on the nZVI (Fig. 5a) [7]. The composites have shown a higher removal capacity of Pb^{2+} than pristine materials, in the entire range of pH, where the removal capacity of Zn–nZVI was higher than 99.0% of the evaluated pH conditions. In the case Mt–nZVI, the sorption of Pb was lower than with Z–nZVI, but this composite became more sensitive to the pH variations.

A more representative method to observe the impact of pH is to consider the variation of this parameter (ΔpH) before and after lead sorption (Fig. 5b) [46]. In the case of Zeolite and nZVI, ΔpH which indicates that the Pb^{2+} sorption process promotes the release of OH^-, whereas in the case of Mt, a diminished pH is obtained as a consequence of the Pb^{2+} sorption [46].

According to the literature, a diminished pH and surface charge favor the formation of monodentate-mononuclear complexes between the substrate and lead, especially with Mt taking into consideration the pH range, whereas Zeolite and nZVI present this effect only for pH > 4.5 [47,48]. In the case of composites, an increase of the pH and surface charge is observed, and therefore the Pb^{2+} is mainly absorbed as a bindetate–mononuclear complex, which is a structure less suitable for desorption [46–48].

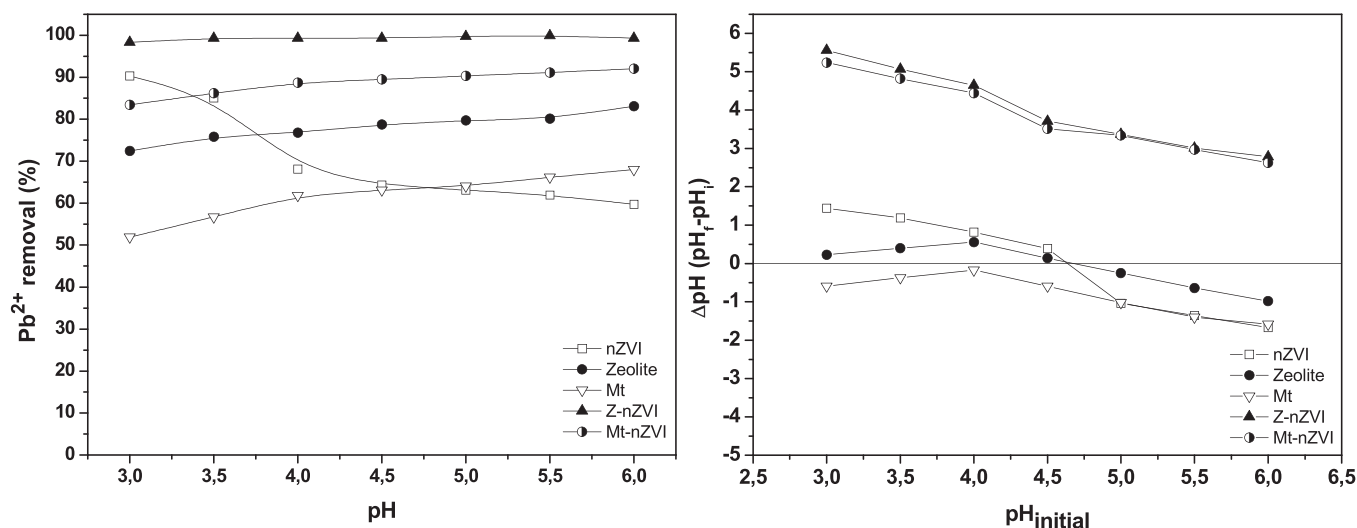**Fig. 3.** Electrophoretic mobility for nZVI, Z, Mt, Z–nZVI and Mt–nZVI.

Fig. 5. (a) Effect of pH on the removal of Pb^{2+} ions on the materials. (b) ΔpH before and after adsorption at different initial pH values.

Table 2
Kinetic parameters predicted from pseudo first and pseudo second-order models. Standard error for each parameter is included in parenthesis.

| Models	Pb				
	nZVI	Zeolite	Mt	Z–nZVI	Mt–nZVI
q_{exp} (mg g^{-1})	48.84	19.98	15.31	79.18	79.70
q_{exp} (%)	61.05	24.97	19.14	99.97	99.62
Pseudo-firstOrder					
q_e (mg g^{-1})	47.25 (0.78)	20.96 (0.11)	14.68 (0.34)	76.8 (0.55)	75.22 (0.27)
k_1 ($x10^{-3}$ min^{-1})	5.93 (0.32)	10.84 (1.27)	13.08 (1.33)	32.60 (1.64)	34.50 (0.08)
r^2	0.99	0.96	0.97	0.95	0.90
R	1.26	0.48	0.20	2.82	10.02
χ^2	0.05	0.05	0.03	0.07	0.27
Pseudo-SecondOrder					
q_e (mg g^{-1})	48.65 (1.86)	19.94 (0.41)	15.32 (0.16)	78.80 (0.91)	78.29 (0.91)
k_2 ($x10^{-3}$ g mg^{-1} min^{-1})	1.19 (0.08)	6.27 0.27)	1.05 (0.03)	8.32 (0.49)	10.08 (0.11)
h(mg g^{-1} min^{-1})	2.82	2.49	0.25	51.66	61.78
r^2	0.99	0.99	0.99	0.99	0.99
R	0.02	0.00	0.00	0.07	0.99
χ^2	0.00	0.00	0.00	0.00	0.03
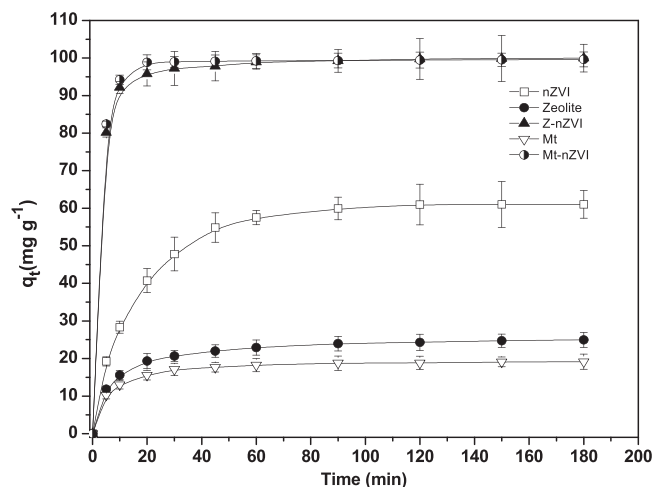
Fig. 6. Effect of the contact time on the removal of Pb^{2+} from each sample.

3.3. Kinetic sorption

Short-term Pb^{2+} removal kinetic data is shown in Fig. 6. The equilibrium time for the removal process of Pb^{2+} shows differ-

ences for pristine and composites materials. In the case of Zeolites, Mt and nZVI, the equilibrium was reached after 90 min, whereas shorter times were obtained for composites, being 20 and 40 min for Mt–nZVI and Z–nZVI, respectively (Fig. 6).

3.4. Pseudo-first order kinetics

By considering the slope and intercept obtained from the log (q_e–q_t) *vs* t (Fig. 7a and Table 2), it is possible to determine the velocity (k_1) and the sorption capacity at equilibrium (q_e). The removal velocities of Pb^{2+} obtained from this model were almost three times higher than with pristine materials, determining the descending sequence Mt–nZVI $\geq$ Z–nZVI > Mt > Z » nZVI. The greater sorption capacity was obtained with composites, being for Z–nZVI, seven times higher than with Zeolite, whereas the sorption capacity (q_e) with Mt–nZVI was 5.1 times higher than with Mt, a behavior already reported in the literature [49–51]. The value of q$_e$, obtained from the linearization of this model was lower than the experimental result (Table 2), indicating that this model has no suitable explanation for the removal of Pb^{2+} from the samples, according to χ^2 and R values and even with high r^2 values. Therefore, the lead adsorption on the samples is not well adjusted to the pseudo first-order kinetics [35,44,52].
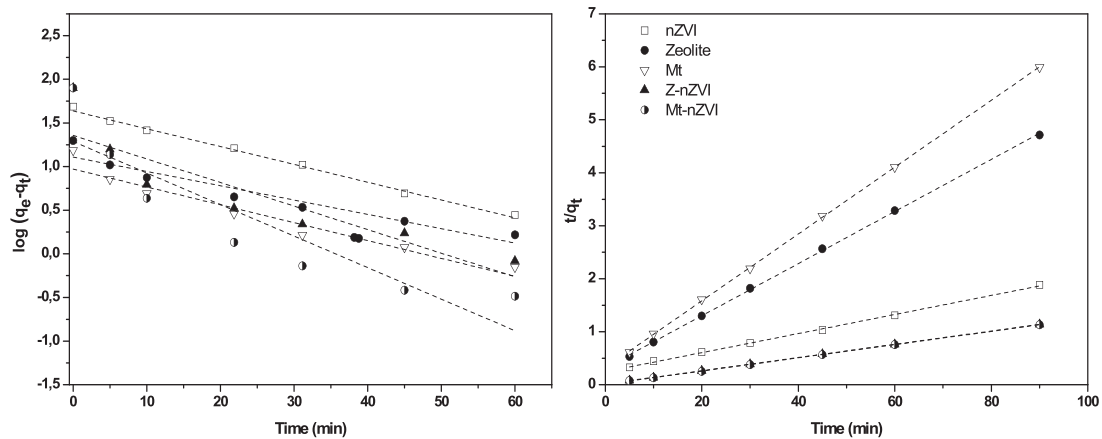
Fig. 7. Pseudo first and second order kinetic model fit for Pb^{2+} sorption onto samples.

Table 3
Intraparticle diffusion coefficients and intercept values for Pb^{2+} adsorption on the samples. Standard error for each parameter is included in parenthesis.

Parameters	Pb				
	nZVI	Zeolite	Mt	Z–nZVI	Mt–nZVI
Intraparticle diffusion					
k_{int-1} (mg g^{-1} min$^{1/2}$)	7.86 (1.07)	3.13 (0.17)	2.21 (0.17)	6.41 (2.38)	6.74 (2.01)
C_1 (mg g^{-1})	4.95 (1.36)	5.45 (0.59)	5.76 (0.58)	68.61 (8.32)	70.00 (7.10)
r^2	0.96	0.99	0.76	0.99	0.82
k_{int-2} (mg g^{-1} min$^{1/2}$)	4.33 (0.90)	0.99 (0.06)	0.51 (0.04)	0.74 (0.17)	0.11 (0.02)
C_2 (mg g^{-1})	24.63 (3.03)	15.31 (0.31)	14.29 (0.26)	93.17 (1.18)	98.35 (0.01)
r^2	0.92	0.99	0.90	0.99	0.92

3.5. Pseudo second-order kinetics

The parameters of the pseudo second-order model, such as the velocity (k_2) and the sorption capacity at equilibrium (q_e) were obtained from the t/q_t *vs* t plot (Fig. 7b, Table 2). This model has shown a high level of adjustment of all of the materials examined, based on the values of r^2, R and χ^2 [2], suggesting that Pb^{2+} removal occurs through a chemical interaction. Similar trends have been reported for the adsorption of Cd^{2+} ions from aqueous solutions by nZVI [2]. In nZVI, Z, and Mt, the equilibrium time was reached after 90 min, while the removal capacity was lower than the composites. A similar behavior has been reported for other adsorbent material and elements [18,49–52].

In the case of Mt–nZVI, the velocity was found to be 10.08 compared to 8.32 obtained for Z–nZVI, showing that the functionalization with nZVI produces a more efficient composite when Mt is used as a template. This result is associated with its expandable structure, favoring the access of Pb^{2+} to the new-formed surfaces [18,35,44,45]. The increase of the surface area could obey the intercalation process that modifies the clay, and is found in the case of Mt with the incorporation of Fe^{3+} during the functionalization and later in the adsorption of Pb^{2+} [23]. An increase of the sorption capacity was also observed for Z–nZVI, however this increase is smaller, compared to the Mt–nZVI composite because Z–nZVI suffers only a slight change in its structure (Table 2).

The initial velocity (h), calculated from the pseudo second order model, shows a similar result as k_2, indicating that during the first stage of contact between the substrate and Pb^{2+} occurs a faster adsorption describing the sequence Mt–nZVI > Z–nZVI > Zeolite » nZVI » Mt.

3.6. Intraparticle diffusion

The differences in structure and textural properties of Zeolite and Mt indicate that it is important to know the adsorption capac-
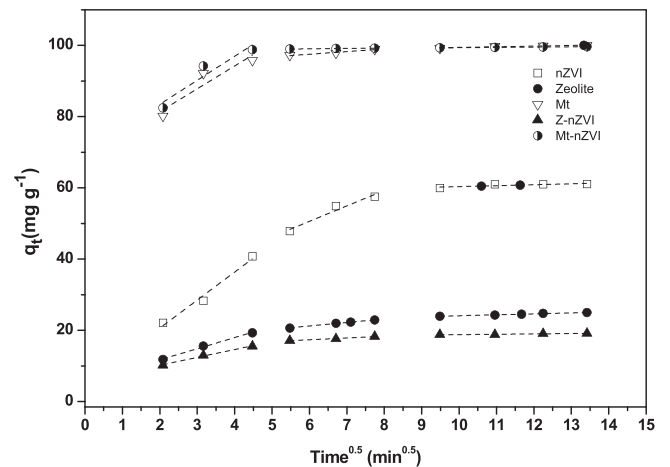

Fig. 8. Intraparticle diffusion plots for Pb^{2+} adsorption on samples.

ity of clays and how this process can be modified as a consequence of the functionalization with nZVI. In order to describe the global velocity of the Pb^{2+} removal, we have applied the Weber–Morris model, used to determine if the intraparticle diffusion is the limiting step of the global velocity for the removal process [2,40] (Fig. 8). If the q_t *vs* $t^{0.5}$ plot presents multi-linearity, then the adsorption can be described in three stages: (1) film or surface diffusion where the sorbate is transported from the bulk solution to the external surface of sorbent; (2) intraparticle or pore diffusion, where sorbate molecules move into the interior of sorbent particles; and, (3) adsorption on the interior sites of the sorbent. From the results applied to this model, we observe multi-linearity in all samples, establishing a removal process of Pb^{2+} controlled by three processes. The main process where Pb^{2+} is sorbed is associated to a surface diffusion (Table 3). After that follows the intra-particle

Table 4
Related parameters for the adsorption of Pb^{2+} on the samples. Standard error for each parameter is included in parenthesis.

Sample	Langmuir			Freundlich		
	K_L	q_{max}	r^2	K_F	n	r^2
nZVI	0.29 (0.02)	50.31 (4.20)	0.99	5.38 (1.03)	3.34 (0.55)	0.90
Zeolite	0.14 (0.02)	68.25 (1.33)	0.99	4.83 (0.61)	2.41 (0.20)	0.97
Mt	0.16 (0.08)	54.23 (1.30)	0.95	4.73 (0.60)	2.76 (0.26)	0.97
Z–nZVI	85.44 (5.71)	105.46 (8.99)	0.95	71.34 (11.47)	3.13 (0.73)	0.76
Mt–nZVI	100.53 (13.36)	115.1 (11.02)	0.97	68.30 (11.46)	3.19 (0.60)	0.86

diffusion, finally reaching the equilibrium (Fig. 8). Differences between the studied materials were observed in the surface diffusion, represented in the first section of Fig. 8, indicating that the structural differences and the functionalization process favor a surface diffusion of Pb^{2+}. In the case of nZVI, this phenomenon was higher than with clays, probably due to the pH condition (5.5), that changes the surface of nZVI and increases the amorphous Fe oxide coating with a high porosity (see Table 1) [43,45]. In the composites, the functionalization with nZVI promotes an increase of the adsorption associated to the surface diffusion, being 8.2 and 7.6 times higher than the results observed for Mt and Zeolites, respectively. The intercept value C is a constant related to the thickness of the boundary layer (Table 3), where larger intercepts suggest that surface diffusion has an important role as the rate-limiting step. This phenomenon was larger in the case of composites, where the heterogeneity of surface groups ($\equiv$Fe—OH, $\equiv$Al—OH y $\equiv$Si—OH) and wide size distribution of porous favor this process. Similar behavior was reported in other investigations [2,18,40].

3.7. Isotherm sorption

The data obtained from sorption isotherms for pristine materials and composites were analyzed with the Langmuir and Freundlich models (Fig. 9). The results of both models applied to the isotherm curves are summarized in Table 4.

The Pb^{2+} sorption is properly described by the Langmuir isotherm (Fig. 9), where a larger sorption is obtained with the composites rather than with pristine materials. The high degree of adjustment between the experimental data and the theory behind the model ($r^2 > 0.99$) suggests that sorption process of Pb^{2+} in Z and nZVI occurs by the formation of monolayers (chemisorptions), whereas for Mt, Mt–nZVI and Z–nZVI (with $r^2 < 0.99$) the removal mechanism can be attributed to physical–chemical processes occurring simultaneously [14,35,45]. The parameters obtained from the Langmuir model show a maximum sorption

capacity (q_m) of Mt–nZVI slightly higher than Z–nZVI, and two times higher than the results for nZVI, Mt and Zeolite (Fig. 9). The functionalization of clays with nZVI has shown a significant change in the sorption intensity, obtained from the Langmuir model (Table 4), where this parameter is 600 times larger than with other substrates. These results can be mainly explained by the structural and surface transformations of the clays, being especially important with Mt. The K_F and n parameters obtained from the Freundlich model have shown a similar tendency with respect to the Langmuir model, indicating that Mt–nZVI exhibits the most efficient removal among all of the all samples, even with a lesser degree of adjustment than Langmuir.

3.8. Clay studied implications on the removal process

The Pb^{2+} sorption in binary systems, like Kaolinite–nZVI and Zeolite–nZVI, were developed by Zhang et al. and Kim et al. [16,17], respectively, showing a similar behavior to our results. Therefore, the removal of Pb^{2+} is clearly favored in clay–nZVI systems, as a consequence of the diminished aggregation and oxidation [16–18].

The functionalization of clays, used as templates, with nZVI, shows no significant effect on the removal parameters obtained from the kinetic and isothermal models. Slightly higher results of equilibrium time and removal capacity were observed with the Mt–nZVI composite. However, the functionalization and later removal processes clearly affected the structure and surface of Mt, compared to those observed with Zeolite. These differences could occur during the functionalization of Mt, where Fe^{3+} is inserted between its layers, increasing the interlaminar space and favoring the ionization of groups with the tendency to release OH^-. Another consequence of this phenomenon can be observed with the XRD and VSM characterizations, where an important presence of iron oxides (magnetite) is found with Mt-nZVI after Pb^{2+} sorption. These results have modified the magnetic response of the composite especially of nZVI [22,35,49–52]. In this context, the nZVI
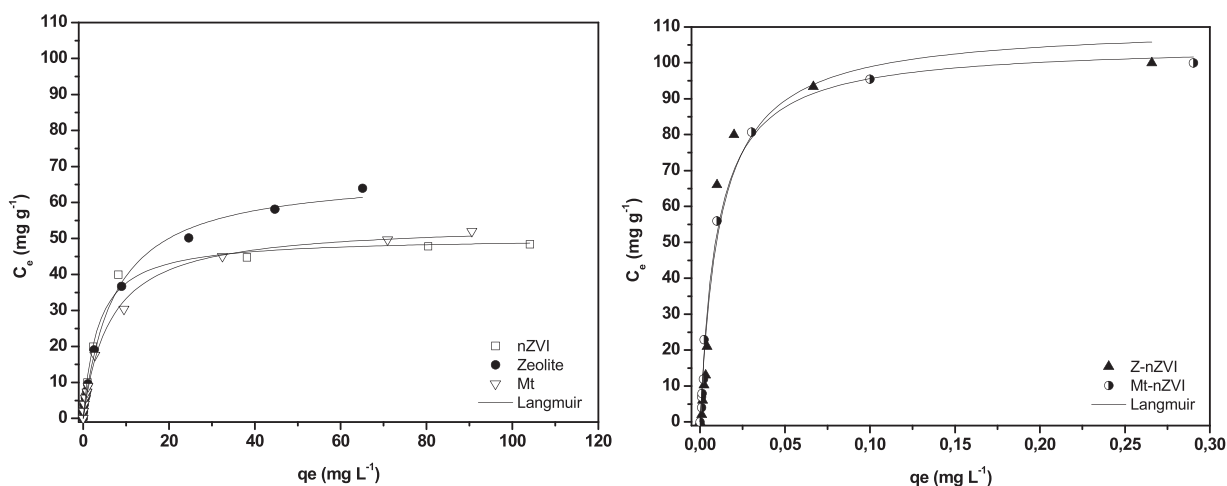
Fig. 9. Adsorption isotherms of Pb^{2+} adsorption on the samples.

used in the Mt–nZVI composite is more likely to follow an oxidation process, due to the intercalation during the Pb^{2+} sorption, where a cation with a larger hydrated radius exposes the nZVI to the environmental oxidizing agents [16,17,22,35].

4. Conclusions

The synthesized composites have shown to be highly effective for the removal of Pb^{2+} compared to pristine materials. Based on their removal capacity and velocity obtained from the isotherm and kinetic studies, the highest efficiency is reached with Mt–ZVI. Furthermore, these results suggest that specific clay plays a critical role in the Pb^{2+} sorption mainly due to the control size of the nZVI embedded in the matrix. After the functionalization process significant changes occur on both clays, being more evident in Mt, where the formation of Fe_3O_4 particles with a larger diameter occurs. The magnetization of both adsorbents indicate the clear presence of Fe and iron oxides being slightly lower in the case of Mt–nZVI/Pb^{2+}, which can be associated with the enhanced formation of iron oxides compared to Zeolites. In general, the shape of the nZVI is found to be spherical, with an aggregation of the particles at specific doping conditions. The enhanced presence of iron oxides occurring specially in Mt reduces the magnetic response of the material whereas the more rigid structure of Zeolite diminishes the formation of thicker iron oxide layers, increasing their magnetic response. The chain-like formation observed in both composites is related to a configuration of minimal energy. This simple preparation method of a magnetic composite, with notably high adsorption ability, opens very interesting perspectives for applying it in many technological applications such as those involving environmental cleaning of polluted water bodies.

Acknowledgments

Appendix A. Supplementary data

Supplementary data associated with this article can be found, in the online version, at http://dx.doi.org/10.1016/j.jhazmat.2015.09.007.

References

[1] D. O'Carroll, B. Sleep, M. Krol, H. Boparai, C. Kocur, Nanoscale zero valent iron and bimetallic particles for contaminated site remediation, Adv. Water Resour. 51 (2013) 104–122.

[2] H.K. Boparai, M. Joseph, D.M. O'Carroll, Kinetics and thermodynamics of cadmium ion removal by adsorption onto nanozerovalent iron particles, J. Hazard. Mater. 1986 (2011) 458–465.

[3] H.R. Dong, X.H. Guan, I.M.C. Lo, Fate of As(V)-treated nano zero-valent iron: determination of arsenic desorption potential under varying environmental conditions by phosphate extraction, Water Res. 46 (2012) 4071–4080.

[4] M. Escudey, J.E. Förster, J.P. Becerra, M. Quinteros, J. Torres, N. Arancibia, G. Galindo, A.C. Chang, Disposal of domestic sludge and sludge ash on volcanic soils, J. Hazard. Mater. 139 (2007) 550–555.

[5] A. Sari, M. Tuzen, Biosorption of cadmium(II) from aqueous solution by red algae (Ceramium virgatum): equilibrium, kinetic and thermodynamic studies, J. Hazard. Mater. 157 (2008) 448–454.

[6] F. Rozada, M. Otero, A. Morán, A.I. García, Adsorption of heavy metals onto sewage sludge-derived materials, Bioresour. Technol. 99 (2008) 6332–6338.

[7] N. Arancibia-Miranda, S.E. Baltazar, A. García, A.H. Romero, M.A. Rubio, D. Altbir, Lead removal bynano–scale zero valent iron: surface analysis and pH effect, Mater. Res. Bull. 59 (2014) 341–348.

[8] F.S. Freyria, B. Bonelli, R. Sethi, M. Armandi, E. Belluso, E. Garrone, Reactions of acid orange 7 with iron nanoparticles in aqueous solutions, J. Phys. Chem. C 115 (2011) 24143–24152.

[9] S. Prado, A. Ulson, Study of lead (II) adsorption onto activated carbon originating from cow bone, J. Clean. Prod. 65 (2014) 342–349.

[10] H. Needleman, Lead poisoning, Annu. Rev. Med. 55 (2004) 209–222.

[11] World Health Organization: Childhood lead poisoning. 2010 <http://www.who.int/ceh/publications/leadguidance.pdf/>.

[12] L. Charlet, Y. Chapron, P. Faller, R. Kirsch, A. Stone, P. Baveye, Neurodegenerative diseases and exposure to the environmental metals Mn, Pb and Hg, Coord. Chem. Rev. 256 (2012) 2147–2163.

[13] I. Dror, O.M. Jacov, A. Cortis, B. Berkowitz, Catalytic transformation of persistent contaminants using a new composite material based on nanosized zero-valent iron, ACS Appl. Mater. Interfaces 4 (2012) 3416–3423.

[14] S.M. Ponder, J.G. Darab, T.E. Mallouk, Remediation of Cr(VI) and Pb(II) aqueous solutions using supported, nanoscale zero-valent iron, Environ. Sci. Technol. 34 (2000) 2564–2569.

[15] W. Wang, M. Zhou, Q. Mao, J. Yue, X. Wang, Novel NaYzeolite-supported nanoscale zero-valent iron as an efficient heterogeneous Fenton catalyst, Catal. Commun. 11 (2010) 937–941.

[16] X. Zhang, S. Lin, Z. Chen, M. Megharaj, R. Naid, Kaolinite-supported nanoscale zero-valent iron for removal of Pb^{2+} from aqueous solution: reactivity, characterization and mechanism, Water Res 45 (2011) 3481–3488.

[17] S.A. Kim, S. Kamala-Kannan, K.J. Lee, Y.J. Park, P. Shea, W.H. Lee, H.M. Kim, B.T. Oh, Removal Pb(II) from aqueous solution by a zeolite-nanoscale zero-valent iron composite, Chem. Eng. J. 217 (2013) 54–60.

[18] N. Arancibia-Miranda, J. Denardin, M. Escudey, M. García-González, C. Pizarro, J. Fabris, L. Charlet, Preparation and characterization of a single-walled aluminosilicatenanotube-iron oxide composite: its applications to removal of aqueous arsenate, Mater. Res. Bull. 51 (2014) 145–152.

[19] S. Wang, Y. Peng, Natural zeolites as effective adsorbents in water and wastewater treatment, Chem. Eng. J. 156 (2010) 11–24.

[20] A. Cincotti, A. Mameli, A.M. Locci, R. Orru, G. Cao, Heavy metal uptake by Sardinian natural zeolites: experiment and modeling, Ind. Eng. Chem. Res. 45 (2006) 1074–1084.

[21] J. Zhu, V. Cozzolino, M. Pigna, Q. Huang, A.G. Caporale, A. Violante, Sorption of Cu, Pb and Cr on Na-montmorillonite: competition and effect of major elements, Chemosphere 84 (2011) 484–489.

[22] Y. Zhang, Y. Li, J. Li, L. Hu, X. Zheng, Enhanced removal of nitrate by a novel composite: nanoscale zero valent iron supported on pillared clay, Chem. Eng. J. 171 (2011) 526–531.

[23] E.G. Garrido-Ramírez, B.K.G. Theng, M.L. Mora, Clays and oxide minerals as catalysts and nanocatalysts in Fenton-like reactions—a review, Appl. Clay Sci. 47 (2010) 182–192.

[24] F. Ji, C.L. Li, B. Tang, J.H. Xu, G. Lu, P. Liu, Preparation of cellulose acetate/zeolite composite fiber and its adsorption behavior for heavy metal ions in aqueous solution, Chem. Eng. J. 209 (2012) 325–333.

[25] A.M. El-Kamash, A.A. Zaki, M. Abed El Geleel, Modeling batch kinetics and thermodynamics of zinc and cadmium ions removal from waste solutions using synthetic zeolite A, J. Hazard. Mater. 127 (2005) 211–220.

[26] P. Tepmatee, P. Siriphannon, Effect of preparation method on structure and adsorption capacity of aluminum pillared montmorillonite, Mater. Res. Bull. 48 (2013) 4856–4866.

[27] J. Musil, J. Blazek, P. Zeman, S. Proksova, M. Sasek, R. Cerstvy, Thermal stability of alumina thin films containing γ-Al2O3 phase prepared by reactive magnetron sputtering, Appl. Surf. Sci. 257 (2010) 1058–1062.

[28] M. Altunlu, S. Yapar, Effect of OH⁻/Al³⁺ and Al³⁺/clay ratios on the adsorption properties of Al-pillared bentonites, Colloids Surf. A: Physicochem. Eng. Aspects 306 (2007) 88–94.

[29] B. Thomas, V.G. Ramu, S. Gopinath, J. George, M. Kunan, G. Laurent, G.L. Drisko, S. Sugunan, Catalytic acetalization of carbonyl compounds over cation (Ce³⁺, Fe³⁺ and Al³⁺) exchanged montmorillonites and Ce³⁺-exchanged Y zeolites, Appl. Clay Sci. 53 (2011) 227–235.

[30] A. Benhammou, A. Yaacoubi, L. Nibou, B. Tanouti, Adsorption of metal ions onto Moroccan stevensite: kinetic and isotherm studies, J. Colloid Interface Sci. 282 (2005) 320–326.

[31] Ç. Üzüm, T. Shahwan, A.E. Eroglu, K.R. Hallam, T.B. Scott, I. Lieberwirth, Synthesis and characterization of kaolinite-supported zero-valent iron nanoparticles and their application for the removal of aqueous Cu^{2+} and Co^{2+} ions, Appl. Clay Sci. 43 (2009) 172–181.

[32] AD, D. att, S.C.L. Fields, arsen, An experimental and computational study of the loading and release of aspirin from zeolite HY, J. Phys. Chem. C 40 (2012) 21382–21390.

[33] M.L. Jackson, Soil Chemical Analysis: Advanced Course, 3th Ed. Madison, 229 Wisconsin, 1969, pp. 894.

[34] S. Azizian, Kinetic models of sorption: a theoretical analysis, J. Colloid. Interface Sci. 276 (2004) 47–52.

[35] W. Yan, M.A.V. Ramos, B.E. Koel, W.X. Zhang, As(III) sequestration by iron nanoparticles: study of solid-phase redox transformations with X-ray photoelectron microscopy, J. Phys. Chem. C 116 (2012) 5303–5311.

[36] W. Rudzinski, W. Plazinski, Kinetics of solute adsorption at solid/aqueous interfaces: searching for the theoretical background of the modified pseudo-first-order kinetic equation, Langmuir 24 (2008) 5393–5399.

[37] Y.-Sh. Ho, Review of second-order models for adsorption systems, J. Hazard. Mater. 136 (2006) 681–689.

[38] Y-S, G.M. Ho, cK, The kinetics of sorption of divalent metal ions onto sphagnum moss peat, Water Res. 34 (2000) 735–742.

[39] C.A. Noubactep, A critical review on the process of con-taminant removal in Fe^0–H_2O systems, Environ. Technol. 29 (2008) 909–920.

[40] M.J.D. Low, Kinetics of chemisorption of gases on solids, Chem. Rev. 60 (1960) 267–312.

[41] L. Cáceres, J. Rodríguez, J. Parra, M. Escudey, L. Barrientos, V. Castro, Sorption kinetics of diuron on volcanic ash derived soils, J. Hazard. Mater. 261 (2013) 602–613.

[42] G. Limousin, J. Gaudet, L. Charlet, S. Szenknect, V. Barthès, M. Krimissa, Sorption isotherms: a review on physical bases, modeling and measurement, Appl. Geochem. 22 (2007) 249–275.

[43] S.E. Baltazar, A. García, A.H. Romero, M.A. Rubio, N. Arancibia-Miranda, D. Altbir, Surface rearrangement of nanoscale zerovalent iron: the role of pH and its implications in the kinetics of arsenate sorption, Environ. Technol. 35 (2014) 1–8.

[44] Y. Xi, M. Mallavarapu, R. Naidu, Reduction and adsorption of Pb^{2+} in aqueous solution by nano-zero-valent iron—a SEM, TEM and XPS study, Mater. Res. Bull. 45 (2010) 1361–1367.

[45] S. Kim, K. Seralathan, K. Lee, Y. Park, P. Shea, W. Leed, H. Kim, B. Oh, Removal of Pb(II) from aqueous solution by a zeolite–nanoscale zero-valent iron composite, Chem. Eng. J. 217 (2013) 54–60.

[46] S. Meng, H. Liu, C. Yang, Y. Wei, D. Hou, Sorption/desorption differences among three ferrihydrites prepared by different synthesis methods, Appl. Surf. Sci. 258 (2012) 4449–4454.

[47] P. Trivedi, J.A. Dyer, D.L. Sparks, Lead sorption onto ferrihydrite. 1. A macroscopic and spectroscopic assessment, Environ. Sci. Technol. 37 (2003) 908–914.

[48] J.A. Dyer, P. Trivedi, N.C. Scrivner, D.L. Sparks, Lead sorption onto ferrihydrite. 2. Surface complexation modeling, Environ. Sci. Technol. 37 (2003) 915–922.

[49] S.R. Kanel, J.M. Greneche, H. Choi, Arsenic(V) removal from groundwater using zero-valent iron as a colloidal reactive barrier material, Environ. Sci. Technol. 40 (2006) 2045–2050.

[50] Y.-Y. Zhang, H. Jiang, Y. Zhang, J.-F. Xie, The dispersity-dependent interaction between montmorillonite supported nZVI and Cr(VI) in aqueous solution, Chem. Eng. J. 229 (2013) 412–419.

[51] S. Bhowmick, S. Chakraborty, P. Mondal, W.V. Renterghem, S.V. Berghe, G.R. Ross, D. Chatterjee, M. Iglesias, Montmorillonite-supported nanoscale zero-valent iron for removal of arsenic from aqueous solution: kinetics and mechanism, Chem. Eng. J. 243 (2014) 14–23.

[52] L. Wu, L. Liao, G. Lv, F. Qin, Stability and pH-independence of nano-zero-valent iron intercalated montmorillonite and its application on Cr(VI) removal, J. Contam. Hydrol. 179 (2015) 1–9.